Title

Selective Down-regulation of KV2.1 Function Contributes to Enhanced Arterial Tone during Diabetes*

Journal

Journal of Biological Chemistry, 290(12)

ISSN

0021-9258

Authors

Nieves-Cintrón, Madeline
Nystoriak, Matthew A
Prada, Maria Paz
et al.

Publication Date

2015-03-01

DOI

10.1074/jbc.m114.622811

Peer reviewed

THE JOURNAL OF BIOLOGICAL CHEMISTRY VOL. 290, NO. 12, pp. 7918–7929, March 20, 2015

Selective Down-regulation of $K_V2.1$ Function Contributes to Enhanced Arterial Tone during Diabetes*

Received for publication, October 30, 2014, and in revised form, January 30, 2015 Published, JBC Papers in Press, February 10, 2015, DOI 10.1074/jbc.M114.622811

Madeline Nieves-Cintrón[‡], Matthew A. Nystoriak[‡], Maria Paz Prada[‡], Kenneth Johnson[‡], William Fayer[‡], Mark L. Dell'Acqua[§], John D. Scott[¶], and Manuel F. Navedo[‡1]

From the [‡]Department of Pharmacology, University of California, Davis, California 95616, the [§]Department of Pharmacology, University of Colorado, Denver, Colorado 80045, and the [¶]Howard Hughes Medical Institute and Department of Pharmacology, University of Washington, Seattle, Washington 98195

Background: K_V channels in vascular smooth muscle cells (VSMCs) regulate arterial tone.
Results: $K_V2.1$ in VSMCs is down-regulated via AKAP150-CaN-dependent NFATc3 signaling during diabetes.
Conclusion: Transcriptional suppression of $K_V2.1$ contributes to enhanced arterial tone in diabetes.
Significance: AKAP150-CaN-dependent activation of NFATc3 may be a general mechanism for transcriptional regulation of K^+ channels, and a valuable target to prevent and treat diabetic vascular complications.

Enhanced arterial tone is a leading cause of vascular complications during diabetes. Voltage-gated K^+ (K_V) channels are key regulators of vascular smooth muscle cells (VSMCs) contractility and arterial tone. Whether impaired K_V channel function contributes to enhance arterial tone during diabetes is unclear. Here, we demonstrate a reduction in K_V-mediated currents (I_{Kv}) in VSMCs from a high fat diet (HFD) mouse model of type 2 diabetes. In particular, I_{Kv} sensitive to stromatoxin (ScTx), a potent K_V2 blocker, were selectively reduced in diabetic VSMCs. This was associated with decreased K_V2-mediated regulation of arterial tone and suppression of the $K_V2.1$ subunit mRNA and protein in VSMCs/arteries isolated from HFD mice. We identified protein kinase A anchoring protein 150 (AKAP150), via targeting of the phosphatase calcineurin (CaN), and the transcription factor nuclear factor of activated T-cells c3 (NFATc3) as required determinants of $K_V2.1$ suppression during diabetes. Interestingly, substantial reduction in transcript levels for $K_V2.1$ preceded down-regulation of large conductance Ca^{2+}-activated K^+ (BK_{Ca}) channel $\beta1$ subunits, which are ultimately suppressed in chronic hyperglycemia to a similar extent. Together, our study supports the concept that transcriptional suppression of $K_V2.1$ by activation of the AKAP150-CaN/NFATc3 signaling axis contributes to enhanced arterial tone during diabetes.

Non-insulin-dependent type 2 diabetes is a devastating disease affecting millions worldwide due to an aging population, sedentary lifestyle, and overnutrition. Vascular dysfunction, including enhanced arterial tone, is a leading cause of cardiovascular complications contributing to morbidity and mortality in the diabetic population (1). Although endothelial dysfunction has long been recognized as a major factor contributing to vascular dysfunction and enhanced arterial tone during diabetes (2–5), abnormal VSMC function may also play a critical role, although the mechanisms for this remain poorly understood. Thus, advances in this area could prove valuable for the development of rational therapies to treat and prevent diabetic vascular complications.

The level of arterial tone is largely determined by vascular smooth muscle cell (VSMC)[2] membrane potential (V_M) and Ca^{2+} entry via voltage-gated, L-type Ca^{2+} channels (LTCCs) (6). A major regulator of V_M is the activity of K_V and BK_{Ca} channels (7–9). Physiological activation of these channels hyperpolarizes VSMCs, thereby decreasing LTCC open probability and Ca^{2+} influx leading to vasodilation, whereas their inhibition promotes vasoconstriction (10). Previous reports have shown that *in vitro*, short term exposure of coronary, cerebral, and mesenteric arteries to extracellular glucose concentrations that resemble diabetic hyperglycemia (*e.g.* 20 mM) inhibit K_V and BK_{Ca} channel activity in VSMCs (11–15). Thus, inhibition of these channels may contribute to enhanced arterial tone and vascular complications during diabetes. Consistent with this, our group and others have found that the activity of BK_{Ca} channels is suppressed in VSMCs of several mouse models of diabetes (14–17). However, whether impaired K_V channel activity in VSMCs contributes to enhanced arterial tone during diabetes is currently unclear.

We recently demonstrated that suppression of BK_{Ca} channel activity in a high fat diet (HFD) mouse model of type 2 diabetes proceeds through activation of the prohypertensive CaN/NFATc3 signaling pathway (14). Activation of NFATc3 required anchoring of CaN by the scaffolding protein AKAP150

* This work was supported by National Institutes of Health Grant R01HL098200 and American Heart Association Grant (AHA) AHA-14GRNT18730054 (to M. F. N.), and NHLBI training grants HL-086350 and HL-07828 and Grant AHA-13POST12730001 and the Lawrence J. and Florence A. DeGeorge Charitable Trust (to M. A. N.). This work was also supported by National Institutes of Health Grant T32GM099608 (to M. P. P.) through the NIGMS.
[1] To whom correspondence should be addressed. Tel.: 530-752-6880; Fax: 530-752-7710; E-mail: mfnavedo@ucdavis.edu.

[2] The abbreviations used are: VSMCs, vascular smooth muscle cells; K_V, voltage-gated K^+ channels; I_{Kv}, K_V currents; V_M, membrane potential; BK_{Ca}, large conductance Ca^{2+}-activated potassium channel; LTCC, L-type Ca^{2+} channels; $[Ca^{2+}]_i$, intracellular Ca^{2+} concentration; AKAP150, A-kinase anchoring protein 150; LFD, low fat diet; HFD, high fat diet; CaN, calcineurin; NFATc3, nuclear factor of activated T cells, c3 isoform; ΔPIX, AKAP150 lacking binding site for calcineurin; ScTx, stromatoxin.

(murine ortholog of human AKAP79) in diabetic cells (14). Considering that this transcription factor is also known to regulate the expression of K_V channels in VSMCs (18), we postulated that activation of this pathway may also modulate K_V function during diabetes.

In the present study, we tested the hypothesis that K_V channel function in VSMCs is impaired and contributes to increased arterial tone in a HFD mouse model of type 2 diabetes, and that the mechanism involves activation of the AKAP150-CaN/NFATc3 signaling pathway. Consistent with this hypothesis, we show that K_V channel function is decreased in VSMCs from wild type (WT) HFD mice due to a reduction in the expression of ScTx-sensitive $K_V2.1$, but not psora-4-sensitive $K_V1.2$ or $K_V1.5$ subunits. Genetic ablation of NFATc3, AKAP150, or disruption of the AKAP150-CaN interaction prevented down-regulation of the $K_V2.1$ subunit, suppression of ScTx-sensitive I_{Kv}, and enhanced arterial tone in HFD mice. Furthermore, our data indicate that down-regulation of $K_V2.1$ occurs at an earlier time point (*i.e.* 1 h) compared with BK_{Ca} $\beta1$ subunits under hyperglycemic conditions. These findings illuminate a critical role for AKAP150-anchored CaN, NFATc3, and $K_V2.1$ function in the regulation of arterial tone during diabetes.

MATERIALS AND METHODS

Animals—WT (C57Bl/6J), AKAP150$^{-/-}$, NFATc3$^{-/-}$, and knock-in mice expressing AKAP150 lacking its CaN binding site (ΔPIX) (19) were euthanized with a lethal dose of sodium pentobarbital (250 mg/kg; intraperitoneally), as approved by the University of California, Davis Institutional Animal Care and Use Committee. Mice were sustained on either a low fat (10% kcal; ct) or high fat (60% kcal) diet (Research Diets, New Brunswick, NJ) starting at 5 weeks of age for 24–26 weeks. The composition of these diets and the propensity of mice maintained on this HFD to develop type 2 diabetes and induce vascular dysfunction of small resistance arteries have been well documented in previous studies (14, 20, 21). Cerebral arteries were used for functional experiments (*i.e.* electrophysiology, arterial diameter, and immunofluorescence), whereas 3rd and 4th order mesenteric arteries were used for electrophysiology experiments in VSMCs from WT LFD and HFD mice and for molecular biology experiments requiring larger tissue samples (*i.e.* Western blots).

Isolation of VSMCs—VSMCs were dissociated from arteries using enzymatic digestion techniques as described previously (18, 22, 23). Middle and posterior cerebral arteries, as well as third and fourth order mesenteric arteries were dissected in ice-cold dissection buffer composed of (in mM): 140 NaCl, 5 KCl, 2 $MgCl_2$, 10 D-glucose, 10 HEPES, pH 7.4, with NaOH. Cerebral arteries were digested in a dissection solution supplemented with papain (1 mg/ml) and dithiothreitol (1 mg/ml) at 37 °C for 7 min, then incubated in dissection buffer supplemented with collagenase type H (0.3 mg/ml) and collagenase type F (0.7 mg/ml) at 37 °C for 7 min. Cells were then washed in ice-cold dissection buffer. Glass pipettes of decreasing diameters were used to gently triturate arteries and obtain single VSMCs. Isolated cells were maintained in ice-cold dissection buffer until use.

Electrophysiology—I_{Kv} from freshly dissociated VSMCs were measured using the conventional whole cell patch-clamp technique with an Axopatch 200B amplifier (Molecular Devices, Sunnyvale, CA). Currents were evoked by 0.6-s depolarizing pulses from a holding potential of −70 mV to +80 (for psora-4-sensitive currents) or to +40 mV (for ScTx-sensitive currents) in increments of +10 mV. A voltage error of 15 mV attributable to the liquid junction potential of the recording solutions used was corrected offline. I_{Kv} were recorded in the continuous presence of the BK_{Ca} channel blocker iberiotoxin (100 nM) to eliminate BK_{Ca} channel activity. Bath solution consisted of the following components (in mM): 120 NaCl, 3 $NaHCO_3$, 4.2 KCl, 1.2 KH_2PO_4, 2 $MgCl_2$, 0.1 $CaCl_2$, 10 D-glucose, and 10 HEPES (pH 7.4). Patch pipette solution was composed of (in mM): 110 K-gluconate, 30 KCl, 0.5 $MgCl_2$, 10 EGTA, 5 HEPES, 5 NaATP, and 1 GTP (pH 7.2 with KOH). Experiments were carried out at room temperature (22–25 °C). Currents were sampled at 20 kHz and low-pass filtered at 5 kHz. Electrophysiology recordings were analyzed using pCLAMP 10.

Quantitative Polymerase Chain Reaction—K_V transcript expression was analyzed in single isolated cells using the Power SYBR Green Cells-to-CT kit (Life Technologies). For these experiments, single VSMCs were collected after enzymatic isolation using a glass micropipette. RT product was used for quantitative PCR. Specific primers to detect $K_V2.1$ (NM_008420; reference number QT00285971), $K_V1.2$ (NM_008417; reference number QT00128100), and $K_V1.5$ (NM_145983; reference number QT00268387) were acquired from Qiagen (Valencia, CA). β-Actin was used as an internal control (GenBank™ accession number V01217; sense nucleotide 2384–2404 and antisense nucleotide 3071–3091). Amplification was performed using a Power SYBR Green PCR cocktail (Life Technologies) and an Applied Biosystems real-time PCR instrument. Expression for each gene was normalized to β-actin and expressed as a percentage of LFD.

Western Blot Analysis—Cerebral and mesenteric arteries were homogenized in a Triton lysis buffer solution containing (in mM) 150 NaCl, 10 Na_2HPO_4, 1 EDTA with 1% deoxycholic acid, 0.1% sodium dodecyl sulfate and protease inhibitors (Complete Mini protease inhibitor cocktail Roche Applied Science), followed by sonication (20 min at 4 °C). Tissue debris and nuclear fragments were removed by centrifugation at 10,000 × *g* (10 min, 4 °C) and whole cell lysates were obtained as the supernatant. An equal amount of protein was loaded for each tissue lysate. Proteins were separated under reducing conditions on a 10% polyacrylamide gel (Bio-Rad) by electrophoresis at 100 V for 1.5 h. Proteins were then electrophoretically transferred to a polyvinylidene difluoride membrane at 20 V (overnight, 4 °C). Membranes were washed in Tris-buffered saline with 0.1% Tween 20 (TBS-T) and blocked with 10% nonfat milk in TBS-T (1 h, room temperature). Membranes were then incubated for 2 h at room temperature with subunit-specific antibodies from NeuroMab (University of California, Davis, Davis, CA). Antibodies and dilutions were as follows: mouse anti-$K_V2.1$ (73-014 clone K89/34; 1:2), anti-$K_V1.2$ (clone 14/16; 1:2), and $K_V1.5$ (clone K7/45; 1:2). Monoclonal antibody against β-actin (MA5–15739; 1:5,000) was from Pierce. Antibodies

were prepared in TBS-T with 1% bovine serum albumin and 0.01% sodium azide. Membranes were then incubated (1 h, room temperature) with horseradish peroxidase-labeled goat anti-mouse (sc-2005; 1:5,000; Santa Cruz) in TBS-T containing 5% nonfat dried milk. Bands were identified by enhanced chemiluminescence and exposure to x-ray film. Densitometry for immunoreactive bands was performed with ImageJ software (National Institutes of Health). β-Actin was used as input control for normalization. Density was expressed as a percentage of control (LFD).

Immunofluorescence—Immunofluorescent labeling of freshly isolated VSMCs was performed as described previously (24) using a monoclonal antibody specific for $K_V2.1$ subunits (NeuroMab; 75-159; clone K39/25, University of California, Davis). The secondary antibody was an Alexa Fluor 488-conjugated donkey anti-mouse (5 mg/ml) from Molecular Probes. Cells were imaged (512 × 512 pixel images) using an Olympus FV1000 confocal microscope coupled with an Olympus ×60 oil immersion lens (NA = 1.4) and a zoom of 3.5 (pixel size = 0.1 μm). Images were collected at multiple optical planes (*z* axis step size = 0.5 μm). The specificity of the primary antibody was tested in negative control experiments in which the primary antibody was substituted with PBS. $K_V2.1$-associated fluorescence was undetected under this experimental condition. Cells for each group were imaged with the same laser power, gain settings, and pinhole for all the treatments.

Arterial Diameter Measurements—Freshly isolated posterior cerebral arteries were cannulated on glass micropipettes mounted in a 5-ml myograph chamber (Living Systems Instrumentation, St. Albans, VT) as described previously (14). Arteries were pressurized to 20 mm Hg and allowed to equilibrate while continuously superfused (37 °C, 30 min, 3–5 ml/min) with physiological saline solution consisting of (in mM): 119 NaCl, 4.7 KCl, 2 $CaCl_2$, 24 $NaHCO_3$, 1.2 KH_2PO_4, 1.2 $MgSO_4$, 0.023 EDTA, and 10 D-glucose aerated with 5% CO_2, 95% O_2. Bath pH was closely monitored and maintained at 7.35–7.40. Following the equilibration period, intravascular pressure was increased to 60 mm Hg and arteries were allowed to develop myogenic tone. Arteries not exhibiting stable myogenic tone after ~1 h were discarded. To assess the contribution of $K_V1.X$ and $K_V2.1$ channel function to regulation of arterial tone, the $K_V1.X$ inhibitor psora-4 (500 nM) and $K_V2.1$ inhibitor ScTx (50 nM), respectively, were added to the superfusate. Arterial tone data are presented as a percent decrease in diameter relative to the maximum passive diameter at 60 mm Hg obtained at the end of each experiment using Ca^{2+}-free saline solution containing nifedipine (1 μM).

Chemicals and Statistical Analyses—All chemical reagents were from Sigma unless otherwise stated. Iberiotoxin was from Peptides International and ScTx-1 was from Alomone Labs. Data are expressed as mean ± S.E. Data obtained using multiple vessels from the same animal were pooled for statistical analyses. Data were analyzed using GraphPad Prism software. Statistical significance was determined by Student's *t* test or one-way analysis of variance followed by Tukey multiple comparison test for comparison of multiple groups. $p < 0.05$ was considered statistically significant (denoted by * in figures).

TABLE 1
Body weight and non-fasting blood glucose in wild type, AKAP150$^{-/-}$, ΔPIX, and NFATc3$^{-/-}$ mice fed low and high fat diet

	Body weight	Blood glucose
	g	*mg/dl*
Wild-type		
LFD	30 ± 0.6	145 ± 4
HFD	42 ± 1.0[a]	301 ± 12[a]
AKAP150$^{-/-}$		
LFD	25 ± 1.1	148 ± 4
HFD	36 ± 3.0[a]	264 ± 16[a]
ΔPIX		
LFD	36 ± 2.0	169 ± 11
HFD	45 ± 1.0[a]	264 ± 24[a]
NFATc3$^{-/-}$		
LFD	32 ± 4.0	147 ± 8
HFD	44 ± 2.0[a]	241 ± 41[a]

[a] Values are mean ± S.E. obtained at 24–26 weeks after start of diet at 5 weeks of age, $p < 0.05$.

RESULTS

Freshly isolated, small diameter (~75–150 μm) cerebral and mesenteric arteries and VSMCs from age-matched mice fed *ad libitum* with either a low fat (LFD, 10% kcal) or high fat (HFD, 60% kcal) diet were used for this study (14, 20). This HFD model of type 2 diabetes was employed because it does not depend on genetic manipulations or chemical destruction of pancreatic β-cells. In addition, it recapitulates clinical features observed in patients with type 2 diabetes (20, 25), including enhanced arterial tone and increased blood pressure (14). WT mice on a HFD had significantly higher average body weight (42 ± 1.0 g) than WT LFD (30 ± 0.6 g; Table 1). Furthermore, non-fasting blood glucose levels were significantly increased in WT HFD (301 ± 12 mg/dl) compared with WT LFD mice (145 ± 4 mg/dl; Table 1).

I_{Kv} Function Is Suppressed in VSMCs from WT Diabetic Mice—Fig. 1 shows I_{Kv} evoked in cerebral VSMCs freshly dissociated from WT LFD and HFD mice in the presence of 100 nM iberiotoxin to inhibit BK_{Ca} channels. The average capacitance of cerebral WT LFD and HFD cells was 19.4 ± 1.2 and 19.0 ± 1.2 pF, respectively ($p > 0.05$). I_{Kv} were initially elicited by 600-ms depolarizing pulses from a holding potential of −85 mV to voltages ranging from −85 to +65 mV in 10-mV increments. We found that the amplitude of control I_{Kv} from WT HFD were significantly lower than that from WT LFD (Fig. 1Ai). Indeed, the current-voltage relationship of control I_{Kv} revealed that current densities were smaller in WT HFD than in WT LFD at most voltages examined (Fig. 1*B*, *i*; $p < 0.05$). At +65 mV, control I_{Kv} were ~42% smaller in WT HFD (21.0 ± 1.8 pA/pF) when compared with WT LFD (36.4 ± 3.5 pA/pF; $p < 0.05$; Fig. 1*B*, *i*). Similar results were observed in mesenteric VSMCs under same experimental conditions (Fig. 1, *B* and *D*, *panel i*, *insets*). These results indicate impaired I_{Kv} in cerebral and mesenteric VSMCs during diabetes.

Impaired Stromatoxin Sensitivity in VSMCs and Arteries from WT Diabetic Mice—Previous studies indicate that $K_V1.2$, $K_V1.5$, and $K_V2.1$ subunits make predominant contributions to I_{Kv} in VSMCs from cerebral and mesenteric arteries (8, 9, 26–28). Thus, we examined whether impaired function of $K_V1.X$- and/or $K_V2.1$-containing channels contribute to suppressed I_{Kv} in VSMCs during diabetes. This was achieved by

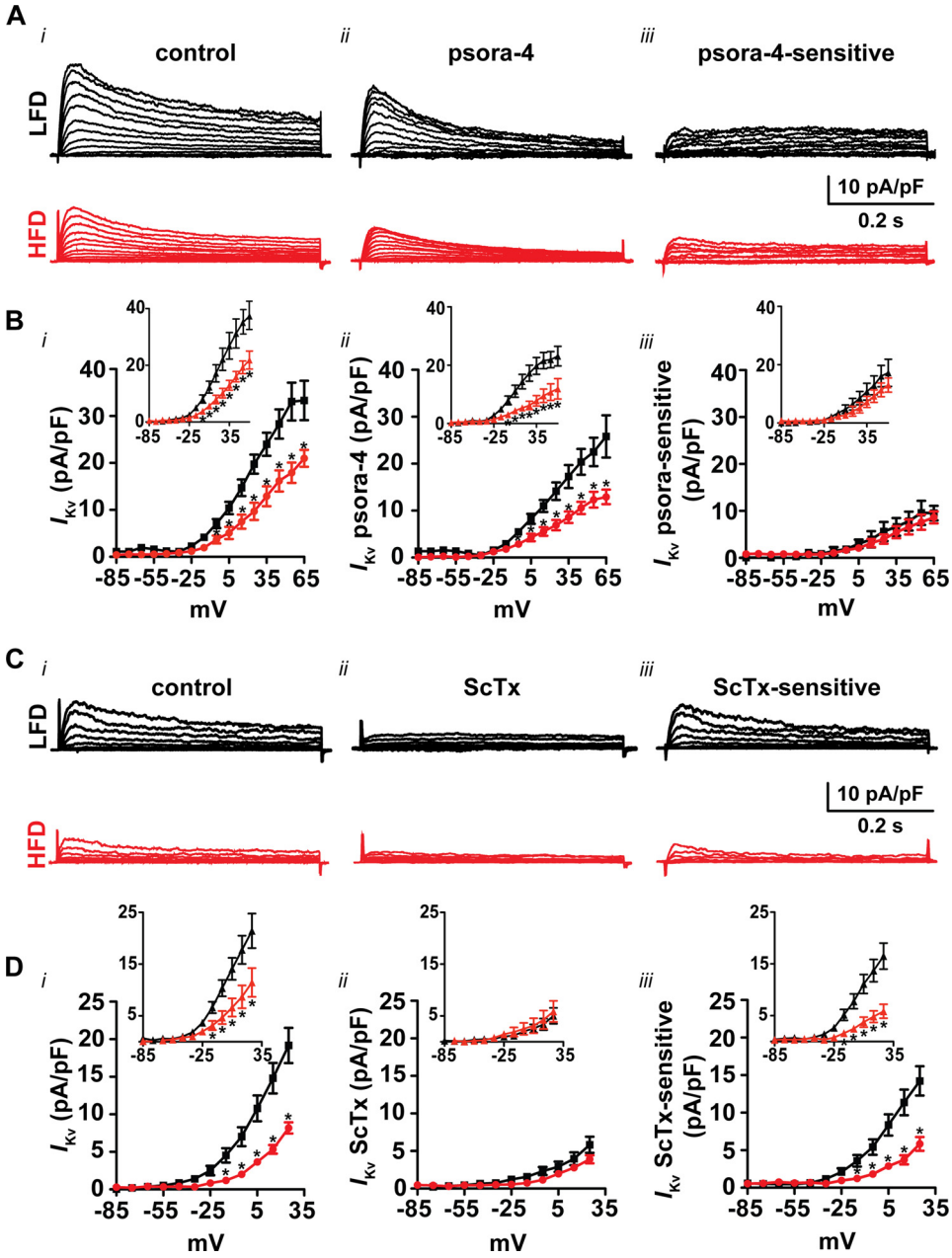

FIGURE 1. **Stromatoxin-sensitive I_{Kv} are suppressed in VSMCs from WT HFD mice.** *A* and *B*, exemplar whole-cell I_{Kv} evoked by depolarizations from −85 to +65 mV and corresponding current-voltage relationships from cerebral and mesenteric (*insets*) LFD ($n = 7$ cerebral cells and 8 mesenteric cells from 5 mice) and HFD ($n = 7$ cerebral and 7 mesenteric cells from 5 mice) VSMCs before (*i*) and after (*ii*) psora-4 (500 nM) application and the resultant psora-4-sensitive component (*iii*). Average capacitance of mesenteric WT LFD and HFD cells is 18.8 ± 1.9 and 19.5 ± 1.5 pF, respectively. Average peak I_{Kv} at +65 mV in LFD and HFD mesenteric cells, respectively, were as follow: control, 37.4 ± 6.0 and 21.8 ± 3.2 pA/pF; +psora-4, 22.7 ± 3.0 and 11.9 ± 3.5 pA/pF; psora-4-sensitive, 17.2 ± 4.0 and 13.0 ± 2.4 pA/pF. *C* and *D*, representative I_{Kv} evoked by depolarization from −85 to +25 mV and the current-voltage relationship from cerebral and mesenteric (*insets*) LFD ($n = 12$ cerebral and 7 mesenteric cells from 7 mice) and HFD ($n = 14$ cerebral and 7 mesenteric cells from 5 mice) cells before (*i*) and after (*ii*) application of ScTx-1 (100 nM) and resultant ScTx-sensitive current (*iii*). Average capacitance of mesenteric WT LFD and HFD cells is 18.8 ± 1.9 and 19.5 ± 1.5 pF, respectively. Average peak I_{Kv} at +25 mV in LFD and HFD mesenteric cells, respectively, were as follows: control, 21.4 ± 3.3 and 11.5 ± 2.8 pA/pF; +ScTx, 5.0 ± 1.5 and 5.9 ± 2.0 pA/pF; ScTx-sensitive, 16.5 ± 2.5 and 5.9 ± 1.3 pA/pF. Psora-4- and ScTx-sensitive components were obtained by digital subtraction of currents in the presence of the specific inhibitor from the currents before application of the inhibitor (control). *, $p < 0.05$.

selectively inhibiting either K_V1 channels with psora-4 (500 nM) (29) or K_V2 channels with ScTx (100 nM) (8, 9). These agents have been used to evaluate the relative contribution of $K_V1.X$ and K_V2 channels in the same VSMCs employed in the present study (8, 9, 30, 31). I_{Kv} were recorded from cerebral VSMCs as described above. The addition of psora-4 decreased I_{Kv} at +65 mV by ~30% in both LFD and HFD VSMCs (Fig. 1*A*, *ii*). However, the amplitude and current-voltage relationship of the psora-4-sensitive I_{Kv} component was similar between these cells (Fig. 1, *A* and *B*, *panels iii*). Inhibition of K_V2 channels with ScTx becomes partial at positive potentials greater than +30 mV (32). Thus, K_V currents were evoked in the presence of ScTx by voltage steps from −85 to +25 mV. Application of ScTx reduced I_{Kv} at +25 mV by ~70% in LFD and ~50% in HFD cells (Fig. 1, *C* and *D*, *panels ii*). Unlike psora-4-senstive I_{Kv}, the amplitude of ScTx-sensitive I_{Kv} was significantly

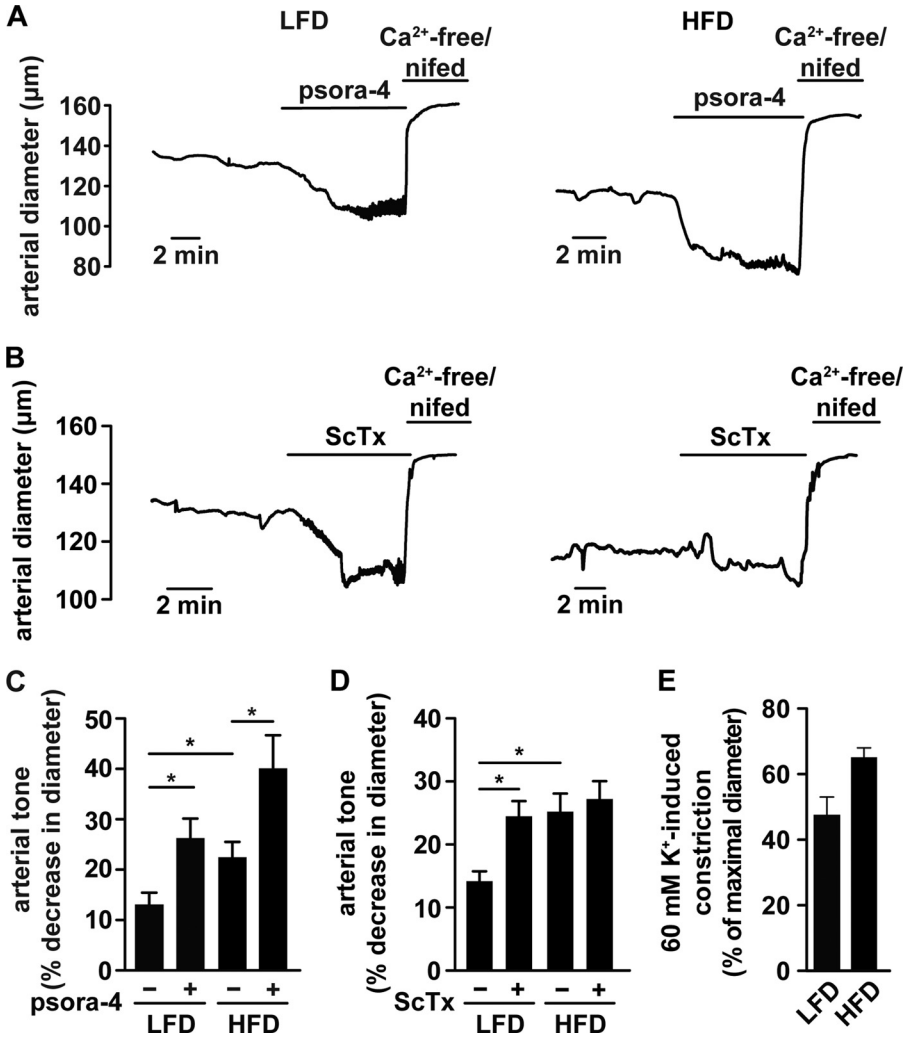

FIGURE 2. **Impaired ScTx-induced constriction in arteries from WT HFD mice.** Representative diameter recordings from pressurized (60 mm Hg) WT cerebral arteries from LFD and HFD mice before and after (*A*) psora-4 (500 nM) or (*B*) ScTx (50 nM). *C*, bar plot summarizing arterial tone in WT LFD ($n = 5$ arteries from 5 mice) and HFD ($n = 5$ arteries from 5 mice) arteries in the absence (−) and presence (+) of psora-4 (*C*). *D*, arterial tone in the absence (−) or presence (+) of ScTx in WT LFD ($n = 7$ arteries from 5 mice) and HFD ($n = 7$ arteries from 6 mice) arteries. *E*, amalgamated data of arterial tone from WT LFD ($n = 8$ arteries from 5 mice) and HFD ($n = 10$ arteries from 5 mice) at 60 mm Hg in response to 60 mM extracellular K^+. *, $p < 0.05$.

smaller across a range of voltages in WT HFD compared with those in WT LFD (5.8 ± 0.9 *versus* 14.2 ± 2.0 pA/pF at +25 mV, respectively; Fig. 1, *C* and *D*, *panels iii*; $p < 0.05$). Similar results were observed in mesenteric VSMCs (Fig. 1, *B* and *D*, *insets*). These data suggest that a reduction in I_{Kv} observed in cerebral and mesenteric VSMCs from HFD mice is due to reduced ScTx-sensitive I_{Kv}.

The functional significance of HFD-associated alterations in I_{Kv} function was assessed by measuring psora-4 and ScTx sensitivity of arterial tone in cerebral arteries from WT LFD and HFD mice. At 60 mm Hg intravascular pressure, WT HFD arteries were significantly more constricted than WT LFD (Fig. 2, *A* and *B*). Whereas application of psora-4 (500 nM) caused a significant constriction in both WT LFD (13 ± 2%) and HFD (17 ± 4%) arteries (Fig. 2, *A* and *C*), ScTx (50 nM) induced constriction only in WT LFD arteries (Fig. 2, *B* and *D*). Indeed, ScTx had little effect on arteries from WT HFD (3 ± 1%) as compared with LFD (11 ± 2%; $p < 0.05$) mice. Arteries from all groups responded with robust constriction to 60 mM extracellular K^+ concentration (Fig. 2*E*) or phenylephrine (14), suggesting that altered ScTx response was not due to differences in the magnitude of tone development. These results are consistent with impaired ScTx-sensitive I_{Kv} contributing to enhanced arterial tone during diabetes.

Down-regulation of $K_V2.1$ Subunits in VSMCs during Diabetes—Impaired sensitivity to ScTx, but not psora-4, in diabetic cells and arteries could reflect selective down-regulation of $K_V2.1$ subunit expression. To test this, we evaluated $K_V1.2$, $K_V1.5$, and $K_V2.1$ transcript levels using quantitative PCR on single isolated cerebral and mesenteric VSMCs from WT LFD and HFD mice. We found that $K_V2.1$ transcript expression was ~65% lower in WT HFD than in WT LFD cells, with no detectable change in the expression of $K_V1.2$ and $K_V1.5$ transcripts (Fig. 3*A*). Consistent with this, $K_V2.1$, but not $K_V1.2$ or $K_V1.5$, protein levels were significantly reduced (~75%) in WT HFD arterial lysates (Fig. 3*B*).

Immunofluorescence was also used to determine changes in $K_V2.1$ subunit expression in isolated cerebral VSMCs from WT LFD and HFD with a $K_V2.1$-specific antibody. As illustrated in Fig. 3*C*, we observed a strong intensity of the $K_V2.1$-associated

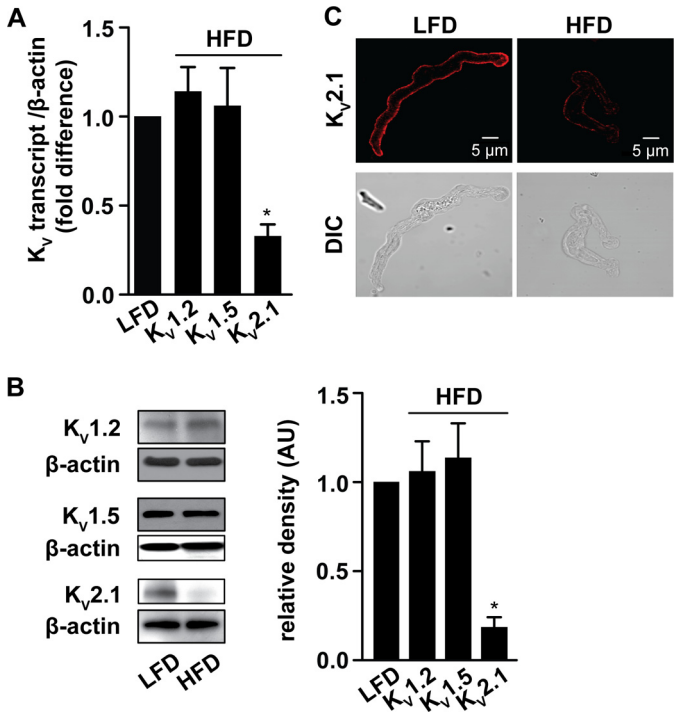

FIGURE 3. **$K_V2.1$ subunit expression is down-regulated in VSMCs and arteries from WT HFD mice.** *A,* bar plot summarizing quantitative real-time PCR data for $K_V1.2$, $K_V1.5$, $K_V2.1$, and KV9.3 transcript levels in WT VSMCs from LFD and HFD mice relative to control (normalized to β-actin; $n \approx 40–50$ VSMCs from 7 mice per condition). *B,* representative blots of immunoreactive bands of expected molecular mass for $K_V1.2$ (~64 kDa), $K_V1.5$ (~66 kDa), $K_V2.1$ (~110 kDa), and β-actin (~43 kDa) (*left*), and corresponding (*right*) densitometry summary data ($n = 4$ lysates per condition). *C,* confocal images of $K_V2.1$-associated fluorescence in WT LFD and HFD VSMCs. *Lower panels* show DIC images for representative cells in the *top panel* ($n = 14$ cells from 3 mice per condition). *, $p < 0.05$.

fluorescence along the sarcolemma of this WT LFD cell. No $K_V2.1$-associated fluorescence was observed when the primary or secondary antibodies were excluded from the preparation. Conversely, the intensity of the $K_V2.1$-associated fluorescence along the sarcolemma, under the same experimental conditions, was markedly lower in cells from WT HFD mice (Fig. 3*C*). Altogether, these data indicate that suppression of ScTx-sensitive I_{Kv} in VSMCs and impaired ScTx-induced vasoconstriction during diabetes results from down-regulation of $K_V2.1$ subunit expression.

AKAP150-anchored CaN and NFATc3 Activity Are Necessary for Impaired ScTx-sensitive I_{Kv} Function and Down-regulation of $K_V2.1$ Subunit Expression during Diabetes—CaN and NFATc3 are known to regulate transcription of $K_V2.1$ in VSMCs (18) and their activity is enhanced in diabetic arteries (14). Activation of CaN and CaN-mediated activation of NFATc3 in VSMCs of diabetic animals is dependent upon sarcolemmal phosphatase targeting by AKAP150 (18, 33). Thus, to test the involvement of this pathway in the suppression of $K_V2.1$ in HFD cells, we first examined the role of AKAP150. To do so, we fed AKAP150-null ($AKAP150^{-/-}$) mice either a LFD or HFD. Non-fasting blood glucose levels and body weight in $AKAP150^{-/-}$ LFD and HFD mice were comparable with corresponding age-matched WT mice, and were elevated in HFD (Table 1).

We measured I_{Kv} in VSMCs from $AKAP150^{-/-}$ LFD and HFD mice before and after ScTx using the voltage protocol described above. VSMCs from $AKAP150^{-/-}$ LFD mice produced robust I_{Kv} (Fig. 4*A*) that were comparable with those observed in WT LFD cells, suggesting that AKAP150 does not influence basal I_{Kv} in VSMCs of control mice. The average capacitance of $AKAP150^{-/-}$ LFD and HFD cells was 17.7 ± 1.2 and 16.4 ± 0.6 pF, respectively, which is similar to WT cells ($p > 0.05$). In contrast to diabetic WT cells, the amplitude of control and ScTx-sensitive I_{Kv} at +25 mV in $AKAP150^{-/-}$ HFD cells (13.0 ± 2.0 pA/pF) was similar to the corresponding $AKAP150^{-/-}$ LFD cells (14.0 ± 2.0 pA/pF; Fig. 4, *A* and *B*). Likewise, no differences in ScTx-insensitive components were observed. Consistent with the electrophysiological data, $K_V2.1$ transcript and protein levels (Fig. 4, *D* and *E*) were similar in cells and lysates, respectively, from $AKAP150^{-/-}$ LFD and HFD mice. Ablation of AKAP150 did not alter basal expression of $K_V2.1$ subunits (Fig. 4*E*). These data indicate that AKAP150 is required for suppression of $K_V2.1$ subunit expression and function in diabetic VSMCs.

Next, we directly tested the role of AKAP150-CaN interactions in $K_V2.1$ suppression during diabetes. To do this, we used VSMCs from LFD and HFD knock-in mice expressing mutant AKAP150 that is unable to bind CaN (ΔPIX) (14, 19). Non-fasting glucose levels and body weight were significantly elevated in ΔPIX HFD compared with ΔPIX LFD mice (Table 1). Selective disruption of the AKAP150-CaN interaction abolished suppression of ScTx-sensitive I_{Kv} function and $K_V2.1$ subunit expression during diabetes (Fig. 4, *C–E*). These results indicate that subcellular targeting of CaN by AKAP150 is necessary for suppression of $K_V2.1$ expression and function in VSMCs during diabetes.

The above findings are consistent with the concept that AKAP150-targeted CaN signals $K_V2.1$ transcriptional suppression via downstream activation of NFATc3. Therefore, we investigated the role of NFATc3 in suppression of $K_V2.1$ expression and function during diabetes by using NFATc3 null ($NFATc3^{-/-}$) mice in LFD or HFD (Table 1). Fig. 5*A* demonstrated that $NFATc3^{-/-}$ LFD and HFD myocytes produced robust I_{Kv}. Consistent with a role for NFATc3, ScTx-sensitive I_{Kv} function and $K_V2.1$ expression (Fig. 5, *A–D*) were similar in VSM and arteries from $NFATc3^{-/-}$ LFD and HFD mice. Together, our data indicate that anchoring of CaN by AKAP150 mediates impairment of $K_V2.1$ expression and function during diabetes via downstream activation of NFATc3.

Loss of AKAP150, AKAP150-targeted CaN, or NFATc3 Prevents Enhanced Arterial Tone and Restores ScTx-sensitive Constriction in Diabetic Mice—We examined the functional relevance of the AKAP150-anchored CaN and NFATc3 signaling module on arterial tone and ScTx sensitivity. Diameter measurements at 60 mm Hg intravascular pressure were performed in cerebral arteries from $AKAP150^{-/-}$, ΔPIX, and $NFATc3^{-/-}$ mice in LFD and HFD. Unlike ScTx observations in arteries from WT mice (see Fig. 2, *B* and *D*), arterial tone development and ScTx-induced constriction were similar in LFD and HFD vessels from $AKAP150^{-/-}$, ΔPIX, and $NFATc3^{-/-}$ mice (Fig. 6, *A–C*). Altogether, these data indicate that disruption of the

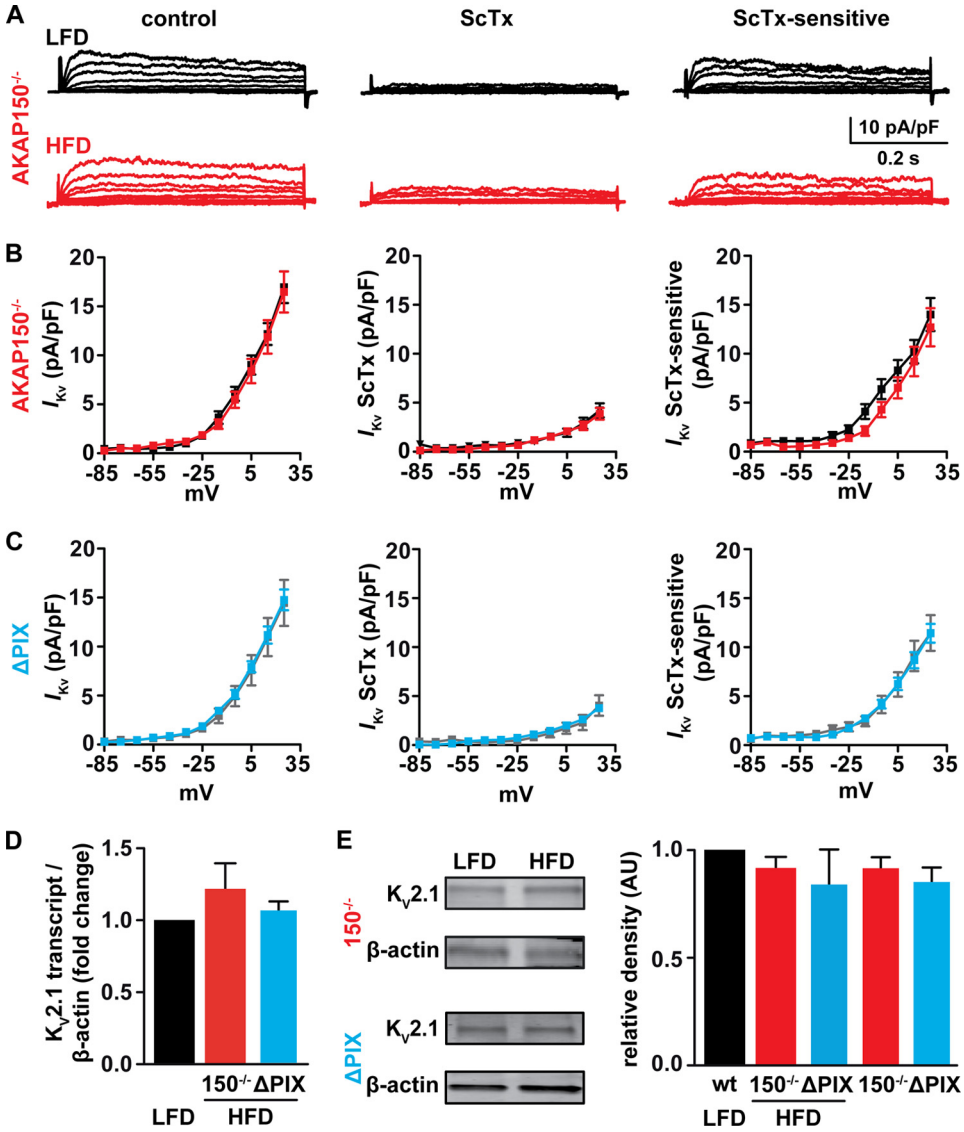

FIGURE 4. **AKAP150-anchored CaN is necessary for impaired $K_V2.1$ expression and function in HFD cells.** *A,* representative whole cell K_V currents from VSMCs isolated from LFD and HFD AKAP150$^{-/-}$ mice recorded before and after application of ScTx (100 nM), and the corresponding ScTx-sensitive component ($n = 11$ cells from 5 LFD mice and 9 cells from 5 HFD mice). Current-voltage relationships of I_{Kv} before and after ScTx and the corresponding ScTx-sensitive component in LFD and HFD (*B*) AKAP150$^{-/-}$ and (*C*) ΔPIX cells. *D,* bar plot of $K_V2.1$ transcript levels in AKAP150$^{-/-}$ and ΔPIX HFD cells relative to LFD normalized to β-actin ($n \approx 40$–50 VSMCs from 3 mice per condition). *E,* Western blot of immunoreactive bands of the expected molecular masses for $K_V2.1$ (~110 kDa) and β-actin (~43 kDa) in control, LFD, and HFD arteries from AKAP150$^{-/-}$ and ΔPIX mice (*left*) and corresponding (*right*) densitometry summary data ($n = 4$ lysates from 4 mice per condition). *, $p < 0.05$.

AKAP150-CaN interaction or ablation of NFATc3 restores normal $K_V2.1$ regulation of myogenic tone during diabetes.

Differential Suppression of $K_V2.1$ and BK_{Ca} β1 Expression at Earlier Stages of Diabetic Hyperglycemia—We further examined the CaN/NFATc3 signaling axis in the suppression of $K_V2.1$ during diabetic hyperglycemia by determining $K_V2.1$ transcript expression in VSMCs from WT arteries incubated for 48 h in medium containing 10 mM D-glucose, 20 mM D-glucose, 20 mM D-glucose + 10 μM CaN inhibitory peptide (a specific CaN inhibitor), and 20 mM D-glucose + 5 μM VIVIT (a selective NFAT inhibitor). These D-glucose concentrations are within the range of observed non-fasting blood glucose levels reported for LFD (5–10 mM) and HFD (20 mM) mice. As expected, 20 mM D-glucose caused >60% reduction in the $K_V2.1$ transcript that was not observed when the non-metabolized L-glucose was substituted for D-glucose or when the CaN inhibitory peptide or VIVIT were present in cultured medium (Fig. 7*A*). These results suggest that activation of the CaN/NFATc3 axis in VSMCs is necessary for transcriptional suppression of $K_V2.1$ during diabetic hyperglycemia.

In a previous study, we found that the regulatory BK_{Ca} β1 subunit in VSMCs is down-regulated via activation of AKAP150-CaN/NFATc3 signaling in hyperglycemic animals on HFD leading to BK_{Ca} channel impairment (14). Considering a potential common mechanism of AKAP150-CaN/NFATc3-induced suppression of K_V and BK_{Ca} channels, an important question to be addressed is whether down-regulation of $K_V2.1$ and BK_{Ca} β1 occurs on a similar time scale in response to hyperglycemic stimuli. To test this possibility, we examined the time course of $K_V2.1$ *versus* BK_{Ca} β1 transcript suppression in

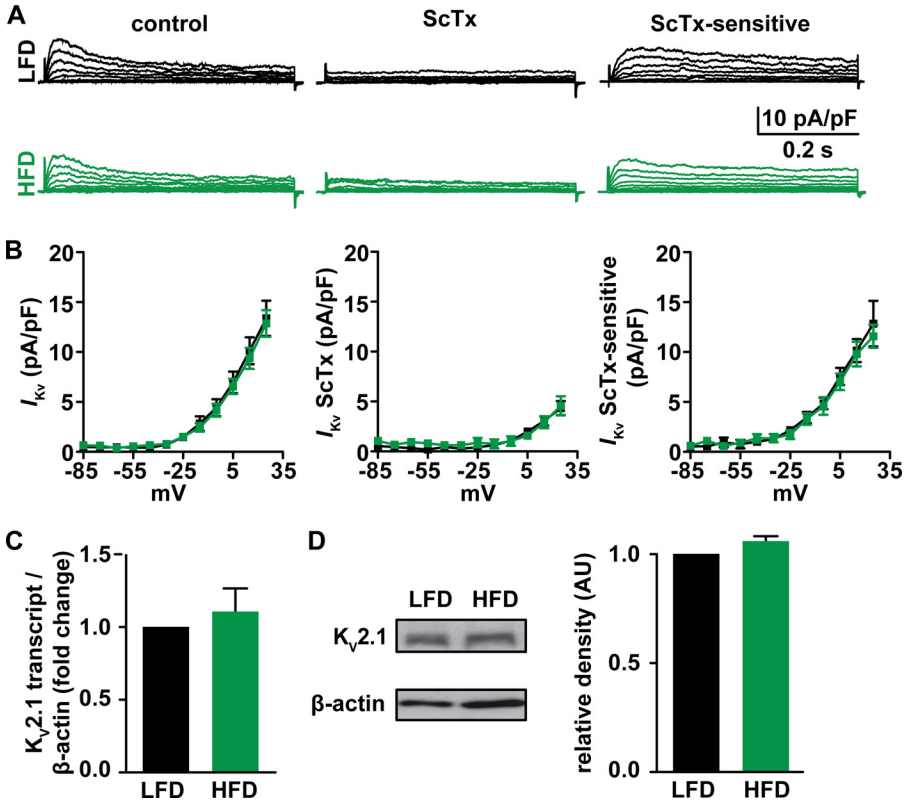

FIGURE 5. **NFATc3 is necessary for down-regulation of $K_V2.1$ expression and function in HFD cells.** *A,* representative whole cell K_V currents from VSMCs isolated from LFD and HFD NFATc3$^{-/-}$ mice recorded before and after application of ScTx (100 nM) and the corresponding ScTx-sensitive component ($n = 6$ cells from 3 LFD mice and 8 cells from 3 HFD mice). *B,* current-voltage relationships of I_{Kv} before and after ScTx and the corresponding ScTx-sensitive component in LFD and HFD NFATc3$^{-/-}$ cells. *C,* bar plot of $K_V2.1$ transcript levels in NFATc3$^{-/-}$ HFD cells relative to LFD normalized to β-actin ($n \approx 40–50$ cells from 3 mice per condition). *D,* Western blot of immunoreactive bands of expected molecular masses for $K_V2.1$ (~110 kDa) and β-actin (~43 kDa) in LFD and HFD arteries from NFATc3$^{-/-}$ mice (*left*) and corresponding (*right*) densitometry summary data ($n = 3$ lysates from 3 mice per condition). *, $p < 0.05$.

VSMCs from WT arteries incubated at different time points in medium containing 10 or 20 mM extracellular D-glucose. We found that increasing the extracellular D-glucose concentration to 20 mM decreased $K_V2.1$ expression by ~60% within the first hour of incubation, but had no effect on BK_{Ca} β1 (Fig. 7*B*). Transcript levels for both genes were subsequently down-regulated to a similar extent after 6, 12, 24, and 48 h in 20 mM D-glucose (Fig. 7*B*). Consistent with a role for AKAP150-anchored CaN in $K_V2.1$ and BK_{Ca} β1 suppression during diabetic hyperglycemia, 20 mM D-glucose had no effect on transcript levels for either gene in VSMCs from ΔPIX mice ($p > 0.05$; Fig. 7*C*). Together, these data suggest a distinct temporal profile of early $K_V2.1$ suppression during diabetic hyperglycemia, with subsequent concomitant down-regulation of both genes to a similar extent that is mediated by direct activation of the AKAP150-anchored CaN/NFAT signaling pathway.

DISCUSSION

In this study, we provide evidence implicating suppression of K_V channel function as a significant contributor of enhanced arterial tone during diabetes (Fig. 7*D*). We report the following novel findings. First, I_{Kv} in cerebral and mesenteric VSMCs are significantly suppressed during diabetes. Second, impaired I_{Kv} in these cells leading to enhanced arterial tone during diabetes occurs due to selective down-regulation of $K_V2.1$ expression. Third, AKAP150-anchored CaN and NFATc3 are obligatory components in the signaling pathway underlying suppression of I_{Kv} and $K_V2.1$ expression during diabetes. Fourth, although $K_V2.1$ and BK_{Ca} β1 transcripts are reduced to a similar extent during established diabetic hyperglycemia, our data suggest that $K_V2.1$ suppression may occur at an earlier stage. The implications of these findings are discussed below.

Considerable data attribute impairment of endothelium-dependent vasodilatory mechanisms as a significant contributor to vascular dysfunction and enhanced arterial tone during diabetes (2–5). However, abnormal VSM function may also critically contribute to enhancement of arterial tone during this pathological condition. For instance, enhanced arterial tone could result from a reduction in outward K^+ conductance in VSMCs (34). Consistent with this idea, our initial experiments demonstrate that K_V channel function is suppressed in diabetic VSMCs (Fig. 1). This discovery is significant, as a reduction in K_V channel function will result in membrane depolarization, and increased activity of LTCCs, ultimately leading to elevated global $[Ca^{2+}]_i$, and VSM contraction (6, 7). Although an increase in global cytosolic $[Ca^{2+}]_i$ could promote activation of BK_{Ca} channels to compensate for the loss of K_V channel function via negative feedback control of V_M depolarization, BK_{Ca} channel activity is also suppressed in WT HFD mice (14). Thus, synergistic impairment of K_V and BK_{Ca} activity in diabetic animals may substantially reduce feedback membrane potential hyperpolarization leading to VSM contraction and enhanced arterial tone during diabetes (Fig. 7*D*). Ultimately, this could

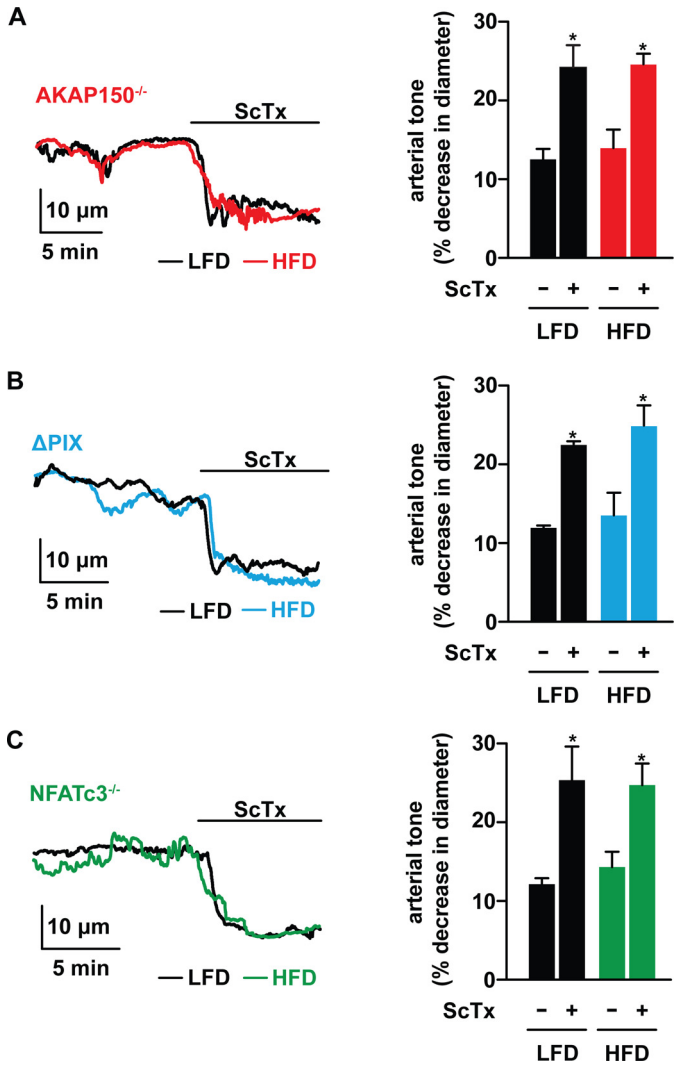

FIGURE 6. **AKAP150-anchored CaN and NFATc3 are necessary for impaired arterial tone in HFD arteries.** Representative diameter recordings (*left panel*) and summary arterial tone data (*right panel*) from pressurized (60 mm Hg) (*A*) AKAP150$^{-/-}$ LFD ($n = 7$ arteries from 5 mice) and HFD mice ($n = 6$ arteries from 4 mice); *B*, ΔPIX LFD ($n = 7$ arteries from 3 mice) and HFD ($n = 8$ arteries from 3 mice), and *C*, NFATc3$^{-/-}$ LFD ($n = 6$ arteries from 3 mice) and HFD ($n = 6$ arteries from 3 mice) cerebral arteries in the absence (−) and presence (+) of ScTx (50 nM). Maximum passive diameters for representative recordings are as follows: AKAP150$^{-/-}$ LFD, 150 μm; AKAP150$^{-/-}$ HFD, 145 μm; ΔPIX LFD, 161 μm, ΔPIX HFD, 154 μm; NFATc3$^{-/-}$ LFD, 153 μm, NFATc3$^{-/-}$ HFD, 155 μm. *, $p < 0.05$ as compared with a minus (−).

significantly contribute to raise mean arterial blood pressure or limit blood flow in diabetic patients.

In this study, we found that psora-4, a selective $K_V1.X$ inhibitor (29–31, 35), induced robust constriction in pressurized arteries from LFD and HFD mice. Yet, ScTx, which is a selective K_V2 inhibitor in VSM (8, 9), had a reduced effect on WT HFD vessels indicating impaired K_V2 channel function during diabetes. Interestingly, we observed a trend toward a greater psora-4-induced constriction in pressurized arteries from WT HFD as compared with WT LFD mice, perhaps reflecting compensatory activation of additional $K_V1.X$ at more depolarized membrane potentials in pressurized arteries from diabetic mice. This difference, however, was not statistically significant. Note that vasoconstriction of cerebral vessels in response to K_V2 or K_V1 channel blockers is independent of functional endothelium (8, 13). Considering this, it follows that reduced endothelial vasodilatory function, as observed in several experimental models of diabetes, would not significantly impact the contribution of K_V2 channels to the regulation of arterial tone. Thus, altered response to ScTx during diabetes observed in this study likely reflects reduced expression of functional K_V2 channels. Consistent with this, ScTx-sensitive and psora-4-insensitive (presumably produced by $K_V2.1$ channels) current densities were significantly suppressed at most membrane potentials in HFD as compared with LFD cells. Conversely, the amplitude of the ScTx-insensitive currents, which presumably are predominantly mediated by $K_V1.X$, and psora-sensitive currents were not different in VSM isolated from LFD and HFD mice. These data indicate that $K_V2.1$, but not $K_V1.X$ channel function is decreased in VSMCs from HFD mice. This conclusion is further supported at the molecular level upon demonstration of reduced $K_V2.1$, but not $K_V1.2$ or $K_V1.5$, transcript and proteins in HFD cells/arteries when compared with LFD cells/arteries. Altogether, these results are the first indication that selective $K_V2.1$ down-regulation underlies reduced I_{Kv} in VSM contributing to enhanced arterial tone during diabetes, and point to impairment of K_V function as a mediator of vascular dysfunction.

An interesting observation in this study is that $K_V2.1$ and BK_{Ca} $\beta1$ genes are differentially suppressed during diabetic hyperglycemia (Fig. 7*B*). Our data indicate that within the first hour of incubation in a hyperglycemic solution that resembles the levels of plasma glucose in HFD mice, $K_V2.1$, but not BK_{Ca} $\beta1$ expression, is significantly down-regulated. Subsequently, concomitant suppression of both genes occurs to a similar extent within 48 h of hyperglycemic exposure. These results suggest that $K_V2.1$ and BK_{Ca} $\beta1$ genes have different thresholds for hyperglycemia-induced transcriptional suppression. Mechanisms of early temporal differences in $K_V2.1$ and BK_{Ca} $\beta1$ expression during hyperglycemic stimuli are unclear, but may involve dissimilar thresholds for NFATc3-dependent suppression or differential mRNA degradation independent of the rate or magnitude of transcriptional suppression (36). Although future studies should further investigate this issue, it is intriguing to speculate that early initiation of $K_V2.1$ suppression could represent a key feature of pre-diabetic hyperglycemia, which drives pathophysiological engagement of the AKAP150-CaN/NFATc3 signaling pathway via membrane depolarization, LTCC activity, and Ca^{2+} influx (37, 38). Subsequently, further NFATc3 nuclear accumulation reaches levels sufficient for BK_{Ca} $\beta1$ down-regulation. Data demonstrating that disruption of the AKAP150-CaN interaction or specific inhibition of CaN and NFAT in VSMCs prevents the down-regulation of $K_V2.1$ and BK_{Ca} $\beta1$ expression (see also Ref. 14) and impaired arterial tone during diabetic hyperglycemia and in HFD gives credence to this hypothesis. However, future experiments should investigate the relationship between NFATc3 activity and $K_V2.1$ and BK_{Ca} $\beta1$ expression in further detail.

Our data support a mechanistic model whereby targeting of CaN by AKAP150 drives NFATc3 activation during diabetes. Once activated, NFATc3 translocates into the nucleus of VSMCs where it reduces $K_V2.1$ and subsequently BK_{Ca} $\beta1$ expression (Fig. 7*D*). Consistent with a critical role for

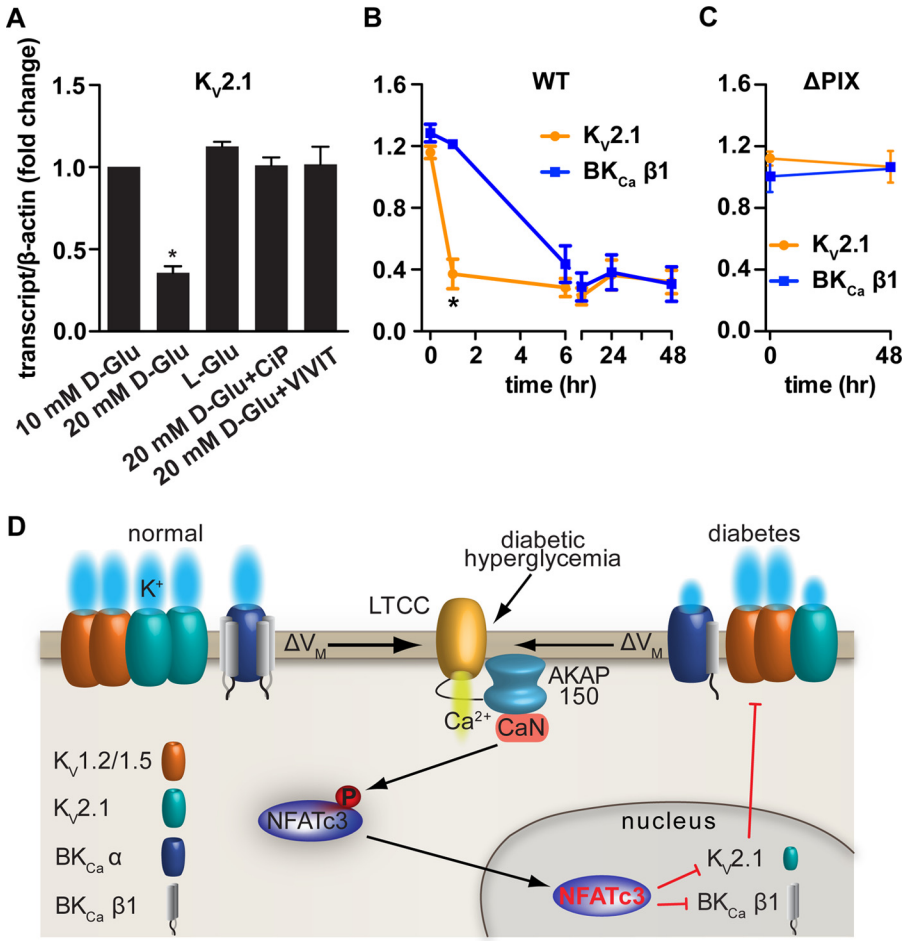

FIGURE 7. **Time course of $K_V2.1$ and BK_{Ca} β1 subunit mRNA expression during diabetic hyperglycemia, involvement of the AKAP150-CaN/NFAT axis, and model for AKAP150-anchored CaN-dependent suppression of K_V and BK_{Ca} subunits during diabetes.** *A*, bar plot of $K_V2.1$ transcript levels in VSMCs from WT arteries incubated in medium supplemented with 10 mM D-glucose, 20 mM D-glucose, 5 mM D-glucose + 15 mM L-glucose, 20 mM D-glucose + 10 μM CaN inhibitory peptide, and 20 mM D-glucose + 5 μM VIVIT ($n \approx 40–50$ cells from 3 mice per condition). Time course of $K_V2.1$ and BK_{Ca} β1 transcripts in WT (*B*) and ΔPIX VSMCs (*C*) following incubation of arteries in 20 mM D-glucose ($n \approx 40–50$ cells from 3 mice per condition). *D*, proposed model for AKAP150-CaN/NFATc3-dependent suppression of K_V and BK_{Ca} channel function in VSMCs during diabetes. *, $p < 0.05$.

AKAP150-anchored CaN, disruption of the interaction between these two proteins prevented NFATc3 dephosphorylation and nuclear accumulation during diabetes (14). This is correlated with restoration of $K_V2.1$ (Figs. 4, 6, and 7) and BK_{Ca} β1 subunit expression and function, and attenuation of blood pressure in diabetic AKAP150$^{-/-}$ and ΔPIX mice (Fig. 7, *B* and *C*, and Ref. 14).

Although our data argue against a role for AKAP150 in basal regulation of K_V or BK_{Ca} channel function (see Figs. 1 and 4 and Ref. 14), this anchoring protein is known to interact with LTCCs (39). Hence, AKAP150 may also function to position CaN near LTCCs (23) to efficiently activate Ca^{2+}-dependent CaN/NFATc3 signaling during diabetes. Indeed, we have previously found that NFATc3 is preferentially activated in VSMCs by LTCC-dependent Ca^{2+} microdomains (*i.e.* Ca^{2+} sparklets (38, 40, 41)), which are significantly elevated during diabetes (42), rather than by elevations in global $[Ca^{2+}]_i$ (40). Similar increases in LTCC-dependent Ca^{2+} microdomains have been observed in angiotensin II-induced hypertensive VSMCs (24, 40) and after activation of reactive oxygen species (43). Thus, increases in local LTCC activity leading to activation of the AKAP-CaN/NFATc3 signaling pathway may represent a wide ranging mechanism for development of vascular dysfunction in many pathological conditions. In the present model, NFATc3 nuclear accumulation and subsequent $K_V2.1$ and BK_{Ca} β1 down-regulation is a dynamic process highly dependent on NFAT nuclear import and export rate (44), as well as non-fasting plasma glucose levels in diabetic animals that could be sufficient for NFAT activation.

In addition to transcriptional suppression of $K_V2.1$ subunit expression, post-translational modification of this (and other K_V) subunit may also contribute to a reduction in I_{Kv} during diabetes (11–13, 45–47). Hence, multiple mechanisms may potentially synergize and contribute to impaired K_V function, and vascular complications during diabetes. Note, however, that activation of divergent mechanisms may vary between vessels and animal models of diabetes. Thus, the relative contribution of transcription-dependent and -independent pathways to altered K_V expression and function during diabetes warrants further investigation.

To summarize, our data demonstrate that suppression of K_V channel function via selective down-regulation of $K_V2.1$ contributes to enhanced arterial tone during diabetes. AKAP150-CaN/NFATc3 signaling is central to impaired $K_V2.1$ expression

and function. Our findings also support the view that activation of this signaling pathway may be a general mechanism for transcriptional regulation of K^+ channels and that with $K_V2.1$, may be novel therapeutic targets to prevent and/or treat vascular complications during diabetes, and perhaps other pathological conditions.

REFERENCES

1. Cooper, M. E., Bonnet, F., Oldfield, M., and Jandeleit-Dahm, K. (2001) Mechanisms of diabetic vasculopathy: an overview. *Am. J. Hypertens.* **14,** 475–486
2. Lagaud, G. J., Masih-Khan, E., Kai, S., van Breemen, C., and Dubé, G. P. (2001) Influence of type II diabetes on arterial tone and endothelial function in murine mesenteric resistance arteries. *J. Vasc. Res.* **38,** 578–589
3. Bagi, Z., Erdei, N., Toth, A., Li, W., Hintze, T. H., Koller, A., and Kaley, G. (2005) Type 2 diabetic mice have increased arteriolar tone and blood pressure: enhanced release of COX-2-derived constrictor prostaglandins. *Arterioscler. Thromb. Vasc. Biol.* **25,** 1610–1616
4. Zimmermann, P. A., Knot, H. J., Stevenson, A. S., and Nelson, M. T. (1997) Increased myogenic tone and diminished responsiveness to ATP-sensitive K^+ channel openers in cerebral arteries from diabetic rats. *Circ. Res.* **81,** 996–1004
5. Sena, C. M., Pereira, A. M., and Seiça, R. (2013) Endothelial dysfunction: a major mediator of diabetic vascular disease. *Biochim. Biophys. Acta* **1832,** 2216–2231
6. Knot, H. J., and Nelson, M. T. (1998) Regulation of arterial diameter and wall [Ca^{2+}] in cerebral arteries of rat by membrane potential and intravascular pressure. *J. Physiol.* **508,** 199–209
7. Knot, H. J., and Nelson, M. T. (1995) Regulation of membrane potential and diameter by voltage-dependent K^+ channels in rabbit myogenic cerebral arteries. *Am. J. Physiol.* **269,** H348–H355
8. Zhong, X. Z., Abd-Elrahman, K. S., Liao, C. H., El-Yazbi, A. F., Walsh, E. J., Walsh, M. P., and Cole, W. C. (2010) Stromatoxin-sensitive, heteromultimeric Kv2.1/Kv9.3 channels contribute to myogenic control of cerebral arterial diameter. *J. Physiol.* **588,** 4519–4537
9. Amberg, G. C., and Santana, L. F. (2006) Kv2 channels oppose myogenic constriction of rat cerebral arteries. *Am. J. Physiol. Cell Physiol.* **291,** C348–C356
10. Nelson, M. T., and Quayle, J. M. (1995) Physiological roles and properties of potassium channels in arterial smooth muscle. *Am. J. Physiol.* **268,** C799–C822
11. Rainbow, R. D., Hardy, M. E., Standen, N. B., and Davies, N. W. (2006) Glucose reduces endothelin inhibition of voltage-gated potassium channels in rat arterial smooth muscle cells. *J. Physiol.* **575,** 833–844
12. Straub, S. V., Girouard, H., Doetsch, P. E., Hannah, R. M., Wilkerson, M. K., and Nelson, M. T. (2009) Regulation of intracerebral arteriolar tone by K(v) channels: effects of glucose and PKC. *Am. J. Physiol. Cell Physiol.* **297,** C788–C796
13. Liu, Y., Terata, K., Rusch, N. J., and Gutterman, D. D. (2001) High glucose impairs voltage-gated K^+ channel current in rat small coronary arteries. *Circ. Res.* **89,** 146–152
14. Nystoriak, M. A., Nieves-Cintrón, M., Nygren, P. J., Hinke, S. A., Nichols, C. B., Chen, C. Y., Puglisi, J. L., Izu, L. T., Bers, D. M., Dell'acqua, M. L., Scott, J. D., Santana, L. F., and Navedo, M. F. (2014) AKAP150 contributes to enhanced vascular tone by facilitating large-conductance Ca^{2+}-activated K^+ channel remodeling in hyperglycemia and *Diabetes mellitus*. *Circ. Res.* **114,** 607–615
15. Zhang, D. M., He, T., Katusic, Z. S., Lee, H. C., and Lu, T. (2010) Muscle-specific f-box only proteins facilitate bk channel $\beta(1)$ subunit down-regulation in vascular smooth muscle cells of diabetes mellitus. *Circ. Res.* **107,** 1454–1459
16. McGahon, M. K., Dash, D. P., Arora, A., Wall, N., Dawicki, J., Simpson, D. A., Scholfield, C. N., McGeown, J. G., and Curtis, T. M. (2007) Diabetes down-regulates large-conductance Ca^{2+}-activated potassium $\beta1$ channel subunit in retinal arteriolar smooth muscle. *Circ. Res.* **100,** 703–711
17. Dong, L., Zheng, Y. M., Van Riper, D., Rathore, R., Liu, Q. H., Singer, H. A., and Wang, Y. X. (2008) Functional and molecular evidence for impairment of calcium-activated potassium channels in type-1 diabetic cerebral artery smooth muscle cells. *J. Cereb. Blood Flow Metab.* **28,** 377–386
18. Amberg, G. C., Rossow, C. F., Navedo, M. F., and Santana, L. F. (2004) NFATc3 regulates Kv2.1 expression in arterial smooth muscle. *J. Biol. Chem.* **279,** 47326–47334
19. Sanderson, J. L., Gorski, J. A., Gibson, E. S., Lam, P., Freund, R. K., Chick, W. S., and Dell'Acqua, M. L. (2012) AKAP150-anchored calcineurin regulates synaptic plasticity by limiting synaptic incorporation of Ca^{2+}-permeable AMPA receptors. *J. Neurosci.* **32,** 15036–15052
20. Winzell, M. S., and Ahrén, B. (2004) The high-fat diet-fed mouse: a model for studying mechanisms and treatment of impaired glucose tolerance and type 2 diabetes. *Diabetes* **53,** S215–S219
21. Kim, F., Pham, M., Maloney, E., Rizzo, N. O., Morton, G. J., Wisse, B. E., Kirk, E. A., Chait, A., and Schwartz, M. W. (2008) Vascular inflammation, insulin resistance, and reduced nitric oxide production precede the onset of peripheral insulin resistance. *Arterioscler. Thromb. Vasc. Biol.* **28,** 1982–1988
22. Nieves-Cintrón, M., Amberg, G. C., Nichols, C. B., Molkentin, J. D., and Santana, L. F. (2007) Activation of NFATc3 down-regulates the $\beta1$ subunit of large conductance, calcium-activated K^+ channels in arterial smooth muscle and contributes to hypertension. *J. Biol. Chem.* **282,** 3231–3240
23. Navedo, M. F., Amberg, G. C., Votaw, V. S., and Santana, L. F. (2005) Constitutively active L-type Ca^{2+} channels. *Proc. Natl. Acad. Sci. U.S.A.* **102,** 11112–11117
24. Navedo, M. F., Nieves-Cintrón, M., Amberg, G. C., Yuan, C., Votaw, V. S., Lederer, W. J., McKnight, G. S., and Santana, L. F. (2008) AKAP150 is required for stuttering persistent Ca^{2+} sparklets and angiotensin II-induced hypertension. *Circ. Res.* **102,** e1–e11
25. Surwit, R. S., Kuhn, C. M., Cochrane, C., McCubbin, J. A., and Feinglos, M. N. (1988) Diet-induced type II diabetes in C57BL/6J mice. *Diabetes* **37,** 1163–1167
26. Albarwani, S., Nemetz, L. T., Madden, J. A., Tobin, A. A., England, S. K., Pratt, P. F., and Rusch, N. J. (2003) Voltage-gated K^+ channels in rat small cerebral arteries: molecular identity of the functional channels. *J. Physiol.* **551,** 751–763
27. Lu, Y., Hanna, S. T., Tang, G., and Wang, R. (2002) Contributions of Kv1.2, Kv1.5 and Kv2.1 subunits to the native delayed rectifier K^+ current in rat mesenteric artery smooth muscle cells. *Life Sci.* **71,** 1465–1473
28. Xu, C., Lu, Y., Tang, G., and Wang, R. (1999) Expression of voltage-dependent K^+ channel genes in mesenteric artery smooth muscle cells. *Am. J. Physiol.* **277,** G1055–G1063
29. Vennekamp, J., Wulff, H., Beeton, C., Calabresi, P. A., Grissmer, S., Hänsel, W., and Chandy, K. G. (2004) Kv1.3-blocking 5-phenylalkoxypsoralens: a new class of immunomodulators. *Mol. Pharmacol.* **65,** 1364–1374
30. Moore, C. L., Nelson, P. L., Parelkar, N. K., Rusch, N. J., and Rhee, S. W. (2014) Protein kinase A-phosphorylated KV1 channels in PSD95 signaling complex contribute to the resting membrane potential and diameter of cerebral arteries. *Circ. Res.* **114,** 1258–1267
31. Kidd, M. W., Leo, M. D., Narayanan, D., Bannister, J. P., and Jaggar, J. H. (2013) Intravascular pressure stimulates functional Kv1.5 surface expression in mesenteric artery smooth muscle cells. *FASEB J.* **27,** 922.3
32. Escoubas, P., Diochot, S., Célérier, M. L., Nakajima, T., and Lazdunski, M. (2002) Novel tarantula toxins for subtypes of voltage-dependent potassium channels in the Kv2 and Kv4 subfamilies. *Mol. Pharmacol.* **62,** 48–57
33. Li, H., Pink, M. D., Murphy, J. G., Stein, A., Dell'Acqua, M. L., and Hogan, P. G. (2012) Balanced interactions of calcineurin with AKAP79 regulate Ca^{2+}-calcineurin-NFAT signaling. *Nat. Struct. Mol. Biol.* **19,** 337–345
34. Jaggar, J. H., Wellman, G. C., Heppner, T. J., Porter, V. A., Perez, G. J., Gollasch, M., Kleppisch, T., Rubart, M., Stevenson, A. S., Lederer, W. J., Knot, H. J., Bonev, A. D., and Nelson, M. T. (1998) Ca^{2+} channels, ryanodine receptors and Ca^{2+}-activated K^+ channels: a functional unit for regulating arterial tone. *Acta Physiol. Scand.* **164,** 577–587
35. Marzian, S., Stansfeld, P. J., Rapedius, M., Rinné, S., Nematian-Ardestani, E., Abbruzzese, J. L., Steinmeyer, K., Sansom, M. S., Sanguinetti, M. C., Baukrowitz, T., and Decher, N. (2013) Side pockets provide the basis for a new mechanism of Kv channel-specific inhibition. *Nat. Chem. Biol.* **9,** 507–513

36. Garneau, N. L., Wilusz, J., and Wilusz, C. J. (2007) The highways and byways of mRNA decay. *Nat. Rev. Mol. Cell Biol.* **8,** 113–126
37. Navedo, M. F., and Amberg, G. C. (2013) Local regulation of L-type Ca^{2+} channel sparklets in arterial smooth muscle. *Microcirculation* **20,** 290–298
38. Nystoriak, M. A., Nieves-Cintrón, M., and Navedo, M. F. (2013) Capturing single L-type Ca^{2+} channel function with optics. *Biochim. Biophys. Acta* **1833,** 1657–1664
39. Oliveria, S. F., Dell'Acqua, M. L., and Sather, W. A. (2007) AKAP79/150 anchoring of calcineurin controls neuronal L-type Ca^{2+} channel activity and nuclear signaling. *Neuron* **55,** 261–275
40. Nieves-Cintrón, M., Amberg, G. C., Navedo, M. F., Molkentin, J. D., and Santana, L. F. (2008) The control of Ca^{2+} influx and NFATc3 signaling in arterial smooth muscle during hypertension. *Proc. Natl. Acad. Sci. U.S.A.* **105,** 15623–15628
41. Navedo, M. F., and Santana, L. F. (2013) CaV1.2 sparklets in heart and vascular smooth muscle. *J. Mol. Cell Cardiol.* **58,** 67–76
42. Navedo, M. F., Takeda, Y., Nieves-Cintrón, M., Molkentin, J. D., and Santana, L. F. (2010) Elevated Ca^{2+} sparklet activity during acute hyperglycemia and diabetes in cerebral arterial smooth muscle cells. *Am. J. Physiol. Cell Physiol.* **298,** C211–C220
43. Amberg, G. C., Earley, S., and Glapa, S. A. (2010) Local regulation of arterial L-type calcium channels by reactive oxygen species. *Circ. Res.* **107,** 1002–1010
44. Gomez, M. F., Bosc, L. V., Stevenson, A. S., Wilkerson, M. K., Hill-Eubanks, D. C., and Nelson, M. T. (2003) Constitutively elevated nuclear export activity opposes Ca^{2+}-dependent NFATc3 nuclear accumulation in vascular smooth muscle: role of JNK2 and Crm-1. *J. Biol. Chem.* **278,** 46847–46853
45. Koya, D., and King, G. L. (1998) Protein kinase C activation and the development of diabetic complications. *Diabetes* **47,** 859–866
46. Ramana, K. V., Friedrich, B., Tammali, R., West, M. B., Bhatnagar, A., and Srivastava, S. K. (2005) Requirement of aldose reductase for the hyperglycemic activation of protein kinase C and formation of diacylglycerol in vascular smooth muscle cells. *Diabetes* **54,** 818–829
47. Hayabuchi, Y., Standen, N. B., and Davies, N. W. (2001) Angiotensin II inhibits and alters kinetics of voltage-gated K^+ channels of rat arterial smooth muscle. *Am. J. Physiol. Heart Circ. Physiol.* **281,** H2480–H2489